J. Fluid Mech. (2021), *vol*. 915, A97, doi:10.1017/jfm.2021.155

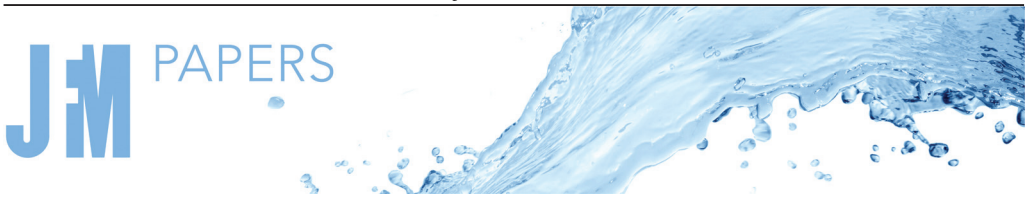

Fluid–structure interactions of a circular cylinder in a stratified fluid

Sarah Christin[1],†, **Patrice Meunier**[1] **and Stéphane Le Dizès**[1]

[1]Aix-Marseille Université, CNRS, Centrale Marseille, IRPHE, 13384 Marseille, France

(Received 20 March 2020; revised 12 January 2021; accepted 16 February 2021)

In this article, the objective is to characterize the influence of a continuous stratification on wake-induced vibrations of a circular cylinder. Experimental results are obtained by towing a horizontal cylinder in a horizontal direction perpendicular to its axes, at a constant speed in a linearly stratified fluid made of salty water. The cylinder can move vertically since it is fixed to free-to-rotate arms. The diameter of the cylinder, the length of the arms and the translating speed are varied. Two flow-induced vibrations modes are observed. The first one is analogous to a vortex-induced vibration (VIV) mode: it is associated with a resonance between the vortex shedding frequency and its frequency is proportional to the natural frequency of the mechanical system, as can be predicted by the VIV theory generalized to low mass ratios. Large amplitude oscillations of the cylinder are found to occur in a large range of velocities also in agreement with the low-mass-ratio VIV theory. The second mode is interpreted as a galloping mode. It has a low frequency and a large amplitude, and occurs for low Froude numbers and long arms. It corresponds to the regimes when the buoyancy forces are larger than the inertial and vertical drag forces. By computing the forces on the cylinder, it is shown that stratification is the source of a destabilizing lift when the cylinder departs from its horizontal motion. Only a weak effect of the Reynolds number on the stability characteristics has been observed in the considered range ($500 < Re < 15\,000$).

Key words: flow–structure interactions, stratified flows, wakes

1. Introduction

Despite the very large number of studies on flow-induced vibrations (FIV), none of them considered the case of horizontal wakes in a stratified fluid. This work aims to characterize the influence of a continuous stratification on wake-induced vibrations of a circular cylinder.

† Email address for correspondence: sarah.christin@univ-amu.fr

Many works have concerned simple geometries such as a circular cylinder that exhibit a large variety of regimes and wake structures. They were initially motivated by applications such as marine cables (Griffin 1985), or taut wires in air (Strouhal 1878). In this civil engineering context, it is important to minimize or control any undesired vibrations that could damage the structure. For other applications, one could instead be interested in increasing the oscillations as they could be a source of energy when coupled to piezoelectric devices (Bernitsas *et al.* 2008; Grouthier *et al.* 2014; Song *et al.* 2015).

As now documented in textbooks (Tritton 2012) and review articles (Williamson 1996*b*), the wake of a cylinder is known to exhibit different regimes as the Reynolds number is varied. As the Reynolds number increases, one observes successively the breaking of the upstream/downstream symmetry, the appearance of a separation bubble (Coutanceau & Bouard 1977), vortex shedding (Von Karman 1911) and a series of three-dimensional transitions (Williamson 1996*a*). One of the most remarkable features is the persistence of the von Kármán vortex street for Reynolds numbers as large as 10^7 (Roshko 1961). These coherent structures induce coherent pressure fluctuations on the cylinder that are responsible for lift and drag fluctuations. When the cylinder is free to move, this induces transverse oscillations (Feng 1968), so-called vortex-induced vibrations (VIV). Reviews can be found in Bearman (1984), Williamson & Govardhan (2004) and Sarpkaya (2004).

VIV have generally been studied experimentally by mounting a circular cylinder on springs in a water channel or a wind tunnel. The system then possesses two reference frequencies:

(i) The frequency f_n associated with the transverse displacement of the structure given by the natural frequency of the springs

$$2\pi f_n = \sqrt{\frac{k}{(m + m_A)}}, \tag{1.1}$$

where k is the spring constant, m the cylinder mass and m_A the potential added mass.

(ii) The frequency f_V associated with vortex shedding given for a fixed cylinder by an empirical formula

$$f_V = St\frac{U}{D}, \tag{1.2}$$

where St is the Strouhal number (Strouhal 1878), U the fluid velocity and D the cylinder diameter. The value of St is found experimentally to be close to 0.2 in a large range of Reynolds numbers $200 < Re < 200\,000$ (Lienhard 1966).

In the classical VIV theory (reviewed by Williamson & Govardhan (2004), for instance) the vortex-shedding frequency is found to synchronize with f_n when f_V reaches f_n (Den Hartog 1954). Both the structure oscillations and vortex shedding then remain locked in at almost a constant frequency in a large interval of velocities. For large mass ratio m^* (equal to the cylinder mass m divided by the mass of an equivalent volume of fluid), this frequency is close to f_n, as observed in the experiments in air performed by Feng (1968) where $m^* = 248$. For small m^* below 20 (Khalak & Williamson 1996, 1997, 1999), this mode of constant lock-in frequency is again observed, called the 'lower branch mode', but with higher amplitudes and a larger frequency compared to high mass ratio experiments. This lock-in frequency non-dimensionalized by f_n has been determined empirically by

Govardhan & Williamson (2000) for a circular cylinder as

$$f^*_{lower} = \sqrt{\frac{m^* + C_A}{m^* - 0.54}}, \tag{1.3}$$

where the added mass coefficient C_A is set to 1. Furthermore, in this low m^* case, a second 'upper branch mode' is observed. It results in oscillations of even larger amplitude than the first mode. The oscillations start when f_V reaches f_n, and have a frequency which grows with the velocity up to f^*_{lower}, where the system switch to the lower branch mode.

Another type of FIV can also come from the breaking of the axisymmetry of the object, it is called galloping. When the object is not circular, a small angle of incidence may induce a destabilizing lift force. This leads to high-amplitude low-frequency oscillations that have been studied for rectangular cylinders (Mannini, Marra & Bartoli 2014), and modified circular cylinder geometries (Nakamura, Hirata & Kashima 1994; Chang, Kumar & Bernitsas 2011). Some studies have also considered the interaction of galloping and vortex shedding (Parkinson & Wawzonek 1981; Mannini *et al.* 2016). Note finally that there exist other FIV phenomena such as buffeting (Blevins 1977), or resulting from the interaction of several objects (Assi, Bearman & Meneghini 2010).

Studies of transverse FIV have considered very complex systems but surprisingly have never tried to include stratification, while most fluids in the environment are stratified. A stably stratified fluid has a density that increases with depth. An important consequence of this is that vertical displacements of fluid parcels are inhibited in stratified flows. Indeed, each fluid parcel is at equilibrium at its initial vertical position and experiences a restoring force if displaced vertically. Following Tritton (2012), let us consider a fluid particle of density $\rho(0)$ that is vertically displaced of a distance Δz. If the adiabatic temperature gradient is negligible, the density of the new surrounding fluid is $\rho(0) + \mathrm{d}\rho/\mathrm{d}z\Delta z$. Then, with the joint association of weight and buoyancy forces, the particle motion is governed by equation

$$\rho(0)\frac{\mathrm{d}^2\Delta z}{\mathrm{d}t^2} = g\frac{\mathrm{d}\rho}{\mathrm{d}z}\Delta z, \tag{1.4}$$

where $\boldsymbol{g}$ is the gravity along the vertical direction z. In a stably stratified fluid, as considered here, the density gradient is negative. This equation then indicates that the particle oscillates around its initial position at the so-called Brünt–Väisälä frequency, N, defined by

$$N^2 = -\frac{g}{\rho(0)}\frac{\partial\rho}{\partial z}. \tag{1.5}$$

This new additional frequency in the system is expected to influence the VIV phenomena described above.

Stratification is already known to modify the wake of a fixed cylinder. As it inhibits vertical motion, it delays the appearance of vortex shedding and narrows the vertical extent of the wake (e.g. Lin & Pao 1979; Honji 1988). It can also be responsible for the appearance of a second vortex-shedding mode when the cylinder is tilted with respect to the horizontal plane (Meunier 2012).

The reference experimental study describing the wake of a horizontal circular cylinder has been carried out by Boyer *et al.* (1989). They have observed 10 different types of regimes as the Reynolds number and the stratification strength are varied. Even more regimes have been found in Chashechkin & Voyekov (1993). Further quantitative studies have been performed since then. Ohya, Uchida & Nagai (2013) measured Strouhal

numbers on various cylinder diameters in wind tunnel experiments with large Reynolds numbers (between 3500 and 12 000). They showed a drastic change of the wake pattern strongly influencing the Strouhal number at a Froude number close to $Fr = U/ND = 2$. Numerically, at low Reynolds numbers, Hwang & Lin (1992) predicted the lift and drag coefficients.

In the present work, we start exploring experimentally the new field of 'stratified wake-induced vibrations' for the simple and most documented geometry of a circular cylinder in a large Reynolds number regime. The objective is to evidence some new phenomena, describe their characteristics and tentatively provide some physical explanations.

The paper is organized as follows. In § 2, the experimental set-up is first described. The main control parameters of the problem are identified. Reference data with a fixed cylinder are also obtained. In § 3, the FIV results are presented. Two oscillation modes are obtained which are successively discussed in §§ 4 and 5. In § 5, some numerical computations are also performed to identify the mechanism of instability. In § 6, the competition between the two modes is further studied, to propose a stability diagram for the system. A brief conclusion is made in § 7.

2. A stratified VIV experiment

2.1. *Facility*

The experimental set-up, sketched in figure 1, consists of a polymethyl methacrylate (PMMA) tank 4 m long, 1 m wide and 1 m deep, which is filled with salty water up to a height H between 70 and 85 cm. A trolley is mounted on rails and moved with a ball screw connected to a motor MAC800 D2 of JVL, allowing a horizontal translation of the system along the tank. The velocity of the trolley is kept constant during each run and varies in the range $1.3 \leqslant U \leqslant 23$ cm s^{-1}.

Three different cylinders of diameter D (equal to 3.2, 4 and 6.2 cm) and length L_y of 63.9 cm are considered. This leads to large ratios $L_y/D > 10$ and $H/D > 12$ which minimizes end effects in the transverse direction y and at the top and bottom of the tank.

As illustrated in figure 1, the cylinder is mounted on flat blade-shaped arms, which are free to rotate around their junction point with the supports thanks to ball bearings. The length L of these arms is an important parameter chosen between 15 and 50 cm.

Using a similar set-up in a homogeneous fluid, De Wilde, Huijsmans & Triantafyllou (2003) considered two spring blade lengths, with an equivalent ratio L/D of 12 and 24. They concluded that the in-line motion of the cylinder and its small rotation did not influence the VIV for oscillation amplitudes below $0.6D$, which are the larger 'VIV' amplitudes we obtain in the present study (see § 4). Even though in our experiments the L/D value can be as low as 2.42, the results did collapse whatever the aspect ratio, which indicates that these effects remain small.

The flat shape of the arms and of their junction with the cylinder, using two screws, limit tilting and minimize the arm-induced drag. Indeed, an estimation of this drag compared to the cylinder drag can be obtained in homogeneous water using the formula for a thin flat plate inclined of an angle θ to the flow, given by Blevins (1984). It shows that, for the angles obtained here (14° at most), and in the 'worst' configuration (i.e. with longer arms and smaller cylinder), both arms induce only approximately 4 % of the cylinder drag. This justifies that arm drag will be neglected in the following. All the parameters of every experiment performed are summarized in table 1.

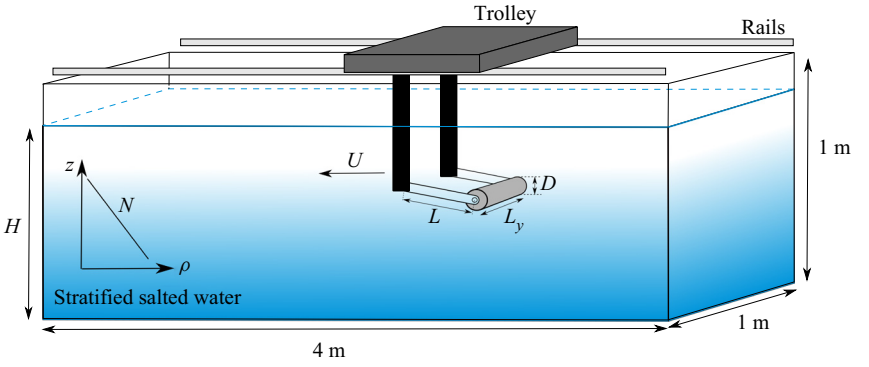

Figure 1. Sketch of the experimental set-up with the main parameters: velocity U, length of arms L, cylinder diameter D and the Brünt–Väisälä frequency N defined by (1.5).

Exp. no.	D (cm)	L (cm)	N (rad s^{-1})	l	Re/Fr	U_0^*	Symbol
1		15	0.4 ± 0.1	2.42	1.54×10^3	17.32	★
2	6.2	30	0.52 ± 0.05	4.84	2.00×10^3	24.50	○
3		50	0.72 ± 0.02	8.06	2.77×10^3	31.62	□
4		15	0.37 ± 0.02	3.75	5.92×10^2	21.57	★
5	4	30	0.62 ± 0.03	7.5	9.92×10^2	30.50	○
6		50	0.65 ± 0.05	12.5	1.04×10^3	39.37	□
7	4	15	0	3.75	0	21.57	★
8		15	0.45 ± 0.1	4.67	4.61×10^2	24.07	★
9		19	0.95 ± 0.01	6	9.69×10^2	27.28	◇
10		30	0.83 ± 0.06	9.38	8.50×10^2	34.12	○
11	3.2	30	0.38 ± 0.05	9.38	3.89×10^2	34.12	○
12		34	1.07 ± 0.15	11	1.09×10^2	36.94	✱
13		45	1.22 ± 0.07	14	1.23×10^2	41.67	+
14		50	0.83 ± 0.06	15.63	8.50×10^2	44.03	□

Table 1. Parameters of the different experimental configurations. For each configuration, approximately 20 different values of the translation velocity are considered between 1.3 and 23 cm s^{-1}. The last column indicates the symbol used for each experiment in the figures.

The damping induced by ball bearings is measured in air using the pendulum model

$$\ddot{\theta} + \frac{c}{m}\dot{\theta} + \omega_0^2\theta = 0, \tag{2.1}$$

with $\omega_0 = \sqrt{g/L} \approx 4.43$ rad s^{-1} for arms of length $L = 50$ cm. The damping coefficient c is found by fitting the exponential decay of the cylinder position over 96 periods, and found to be $c = 5.6 \pm 0.2 \times 10^{-3}$ kg s^{-1} (for a cylinder of mass $m = 525 \pm 0.1$ g in this experiment). It corresponds to a damping ratio $\zeta = c/2m\omega_0 = 1.20 \pm 0.05 \times 10^{-3}$.

The mass m of the cylinder is adjusted within 1 % so that it is at equilibrium when the arms are roughly horizontal. This was done by adding (respectively removing) mass from inside the hollow cylinder, and by using steel (respectively plastic) screws. The uncertainties are such that, at rest, the cylinder is at 50 ± 4 cm from the bottom of the tank.

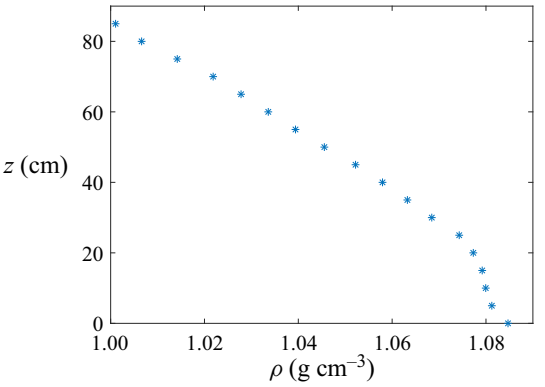

Figure 2. Plot of the density profile two days after the creation of the stratification. By taking $\rho_0 = \rho\ (z = 50\ \text{cm}) = 1.046\ \text{g cm}^{-3}$ as density reference, one can find $N = 1.06\ \text{rad s}^{-1}$.

2.2. *Stratification*

The tank is filled with salty water with a salt concentration increasing linearly with depth. The fluid density can be written as $\rho = \rho_0(1 - zN^2/g)$, where ρ_0 is the density at the cylinder equilibrium position.

This stratification is obtained using a technique described in Bosco (2015). It consists of dividing the tank into two parts, one with pure water and the other one with uniformly mixed strongly salty water, and letting the two fluids mix through holes of diameter 0.5 cm drilled in the separation slab. This technique is preferred to the usual 'two tanks method' because it requires only one tank, which is far more convenient considering the huge volume used here.

A plot of the density profile just after the stratification creation is shown in figure 2. One can notice that the profile is linear from $z = 20$ cm to the free surface at $z = 85$ cm, but a mixed layer is observed for $z < 20$ cm. This is due to a stronger mixing occurring at the bottom when the salty and pure water blend through the slab holes. We have been able to limit this effect that could also happen at the free surface by closing some of the holes.

Experiments are typically performed during a few months with the same water. During this period, the value of N decreases progressively owing to leaks and the mixing generated by the displacements of the cylinder. In order to minimize these effects, the tank is regularly filled with fresh water at the top and/or salty water at the bottom. Every experimental day, a density profile is measured to recompute N, but mixing still induces uncertainties on N from 2 % up to 25 % for the runs with the largest cylinder diameter and the strongest oscillations.

2.3. *Important non-dimensional parameters*

From the geometrical parameters (D, L, H, L_y), as defined in figure 1, the translation speed U and the fluid properties (kinetic viscosity ν, diffusion coefficient $\mathcal{D}$ and N), an important number of non-dimensional parameters can be defined:

(i) the Reynolds number $Re = UD/\nu$;
(ii) the Froude number $Fr = U/ND$;
(iii) the length ratio $l = L/D$;
(iv) the Schmidt number $Sc = \nu/\mathcal{D}$;

(v) the mass ratio $m^* = m/(\rho_0 L_y \pi D^2/4)$;
(vi) the geometric ratios L_y/D and H/D.

The last two ratios are large. For this reason, end effects as well as boundary effects associated with the free surface, side and bottom walls are assumed to be negligible. They are not considered in the present study. The Schmidt number is close to $Sc \approx 625$ obtained for $\nu = 10^{-6}$ m^2 s^{-1} and $\mathcal{D} = 1.64 \times 10^{-9}$ m^2 s^{-1}. The mass ratio m^*, is here always equal to 1, which is considered as a very low mass ratio in usual VIV experiments (Khalak & Williamson 1997, 1999).

In the present study, the three important parameters are then Re, Fr and l. They will be varied in the following ranges: $500 < Re < 15\,000$; $0.5 < Fr < 19$; $2 < l < 16$. Of interest is also the ratio Re/Fr that remains constant for each experiment number indicated in table 1. Except for the non-stratified case (experiment number 7), this ratio is large, indicating the dominance of buoyancy over viscous effects.

2.4. *Measurements with fixed cylinder: the Strouhal number*

The Strouhal number, defined in (1.2), corresponds to the non-dimensional frequency associated with vortex shedding for a fixed cylinder. There are only a few data for the Strouhal number law in a stratified fluid. For this reason, experiments with a fixed cylinder are first performed in order to find the Strouhal number dependence in the set-up.

Three different cylinders of diameter $D = 2.1$, 3.1 and 4.1 cm are considered. The measurements were made by analysing the wake patterns in the last two metres of the cylinder course with a shadowgraph method using a camera Sony $\alpha 7s$ taking 25 frames per second, and lens FE 2.8/50 MACRO. This visualization technique reveals regions of the flow where the second derivative of the density field with respect to the isopycnal's normal is positive or negative.

Observed patterns are qualitatively described in Boyer *et al.* (1989), who compiled 10 different regimes in the Fr–Re plane. Figure 3 shows a comparison between their results and the present study. A wave regime is present at low Froude numbers, as the stratification is strong (denoted as single and multiple centreline structures by Boyer *et al.* 1989). Lee waves develop behind the cylinder, due to the oscillatory motion of fluid parcels initially forced to move in the vertical direction by the cylinder passing. The existence of a blocking region ahead of the cylinder can also be observed. It is typical of strongly stratified fluids: see for example Graebel (1969) for the theory, Browand & Winant (1972) for the first experiments, the book of Tritton (2012) or the review of Lin & Pao (1979) for a comprehensive description of the phenomenon. With increasing Fr, the flow starts to separate behind the cylinder and eddies develop. The quite remarkable regime of isolated mixed regions is characterized by a first wake narrowing after the recirculation zone, followed by a localized expansion around a closed mixed region. It is also interesting to note that Boyer *et al.* (1989) showed that this mixed region is dynamic: its streamwise location as well as its thickness depend on time, and oscillate. The last wake pattern presented here looks like a usual turbulent vortex-shedding state. In this so-called turbulent vortical structure regime, the stratification is too weak to prevent the formation of vortices, but it tends to delay their formation and reduce the wake expansion (especially visible on Boyer's picture).

The frequency was measured and dimensionalized to obtain the Strouhal number. Results are plotted in figure 4 as a function of the Froude number, which offers the best collapse.

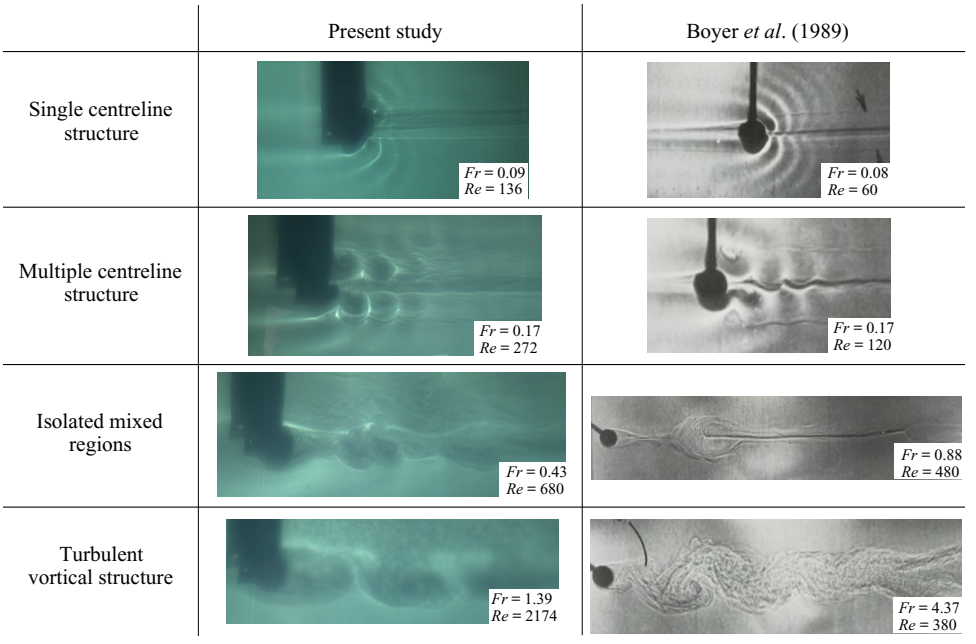

Figure 3. Wake patterns observed by shadowgraph compared to those presented by Boyer *et al.* (1989). For more precision about the regimes and their relative position in the *Fr*–*Re* plane, see Boyer *et al.* (1989).

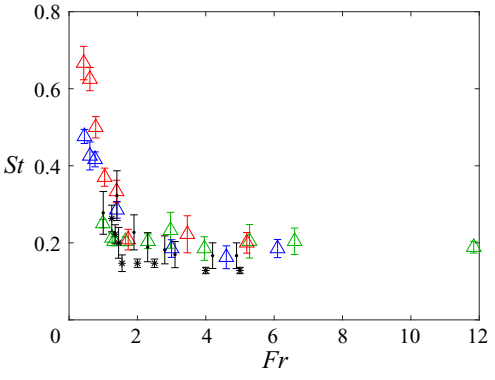

Figure 4. Strouhal number as a function of the Froude number. $D = 2.1$ cm (green), $D = 3.1$ cm (blue) and $D = 4.1$ cm (red). Black symbols stand for experimental (stars) and numerical (dots) results of Meunier (2012) ($Re \in [40, 200]$).

The Reynolds number is equal to $Re = 410\,Fr$ for $D = 2.1$ cm, to $Re = 894\,Fr$ for $D = 3.1$ cm, to $Re = 1563\,Fr$ for $D = 4.1$ cm. The Reynolds number ranges from 400 to 8000 in these experiments. On this plot is also displayed the experimental and numerical results obtained by Meunier (2012) for lower Reynolds numbers ($40 < Re < 200$). This figure clearly shows that the usual value $St \approx 0.2$ of the homogeneous case remains valid here as soon as $Fr > 1.5$.

For lower *Fr*, a sudden increase of the vortex-shedding frequency is observed, in agreement with the numerical and experimental results of Meunier (2012) and Ohya *et al.* (2013). We can also see that this increase becomes larger when the diameter of the cylinder

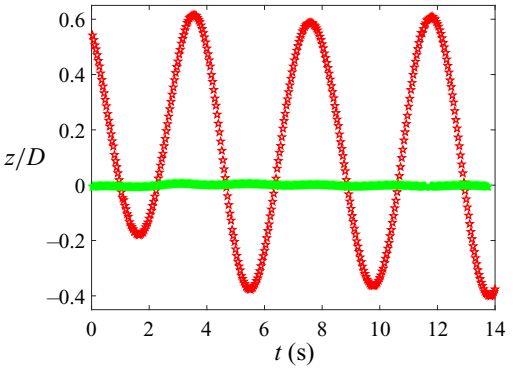

Figure 5. Vertical position of the cylinder in a homogeneous flow (green) and in a weakly stratified flow with $N = 0.37 \pm 0.02$ rad s^{-1}, $Fr = 6.16$ (red). Measurements are for experiment numbers 7 and 4 of table 1, at $Re = 4158$.

is increased for a fixed Fr. This means a growth of the Strouhal number with the Reynolds number for small fixed Fr. This tendency is in agreement with the results obtained by Chashechkin & Voyekov (1993) who observe a linear increase of St with Re for small Froude numbers.

2.5. *Measurements with oscillating cylinder and sources of uncertainty*

As for the fixed cylinder, FIV measurements were performed in the last two metres of the cylinder course with the same apparatus. This means that, when entering the record area, the cylinder was already towed on approximately two metres. Oscillations then started to settle (this can be seen in figure 5 for example).

The software Tracker, a video analysis tool, is capable of following the positions of the ball bearing and of the cylinder. To do so, the user needs to manually target the interesting point on the first image and define a surrounding zone. The software compares the surrounding zone pixel pattern with reduced areas of the next image, to find the best correlation. This method is accurate up to a few pixels (video quality is the main limitation). It induces an error of the order of a millimetre, negligible in this study. The oscillations of the cylinder are then deduced from the calculated angle θ made by the cylinder–ball bearing line with respect to the horizontal. Amplitude A and frequency f are obtained from a least squares fit of the time variation of the angle.

Sources of uncertainties coming from the visualization method or the stratification measurement for instance, are numerous. A few of them can be quantified.

Uncertainties on the Froude number Fr come from the variation of N due to mixing. As already mentioned (§ 2.2), they are mostly lower than 7 % although they can reach 20 % to 25 %, like in experiments 1 and 8 (see table 1).

Uncertainties on the Reynolds number Re of approximately 10 % are mainly due to temperature variation, which modifies the value of the kinematic viscosity.

Uncertainties on the oscillation frequency and amplitude measurement are of order 10 and 15 % for the higher-frequency mode (see § 4), mainly due to the limited number of observed oscillations. For the low-frequency mode, they are of order 5 % (up to 10 % for frequency and to 15 % for amplitude measurements in low-amplitude experiments).

The overall uncertainty present in the measurements is well represented by the scatter in the figures. Although this scatter is important, it is much smaller than the variation of the

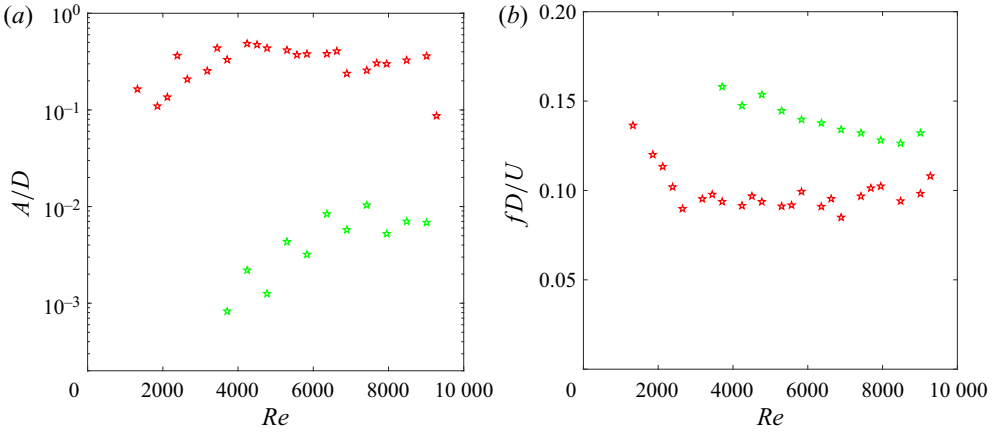

Figure 6. Amplitude (*a*) and frequency (*b*) of the cylinder oscillations as a function of the Reynolds number in a stratified (red) and homogeneous (green) fluid for experiment numbers 7 and 4. In the stratified case, $N = 0.37 \pm 0.02$ rad s^{-1} and Fr varies from 1.8 for the smaller Reynolds number, to 12.6 for the larger one.

amplitude and of the frequencies by a factor of approximately 10 in the range considered in this paper. These quantitative data are thus sufficient to draw convincing conclusions.

3. Effects of stratification

3.1. *Comparison to homogeneous fluid*

Videos of the cylinder moving through the tank were analysed to deduce the evolution of vertical position z of the cylinder as a function of time. A plot of these raw data, in a homogeneous and a stratified fluid, for fixed l and Re, is shown in figure 5. Note that the initial time $t = 0s$, corresponds to the time at which the cylinder enters the camera's field of view. For this reason, the cylinder is not necessarily at the reference position $z = 0$ at $t = 0$.

Figure 5 shows clearly that the cylinder exhibits strong oscillations in a stratified fluid whereas the oscillations are almost undetectable in a homogeneous fluid. This is a first indication that stratification strongly affects the flow-induced vibrations of a cylinder.

Measurements of the amplitude and frequency of the cylinder oscillations are reported in figure 6 as a function of the Reynolds number for the homogeneous and stratified cases. It confirms that, although oscillations are observed in both cases, their amplitudes in stratified water are more than one decade higher than in a homogeneous fluid. Their frequencies non-dimensionalized by U/D are approximatively constant but they are larger in the homogeneous case.

3.2. *The existence of two vibration modes*

The stratified experiments were repeated with different speeds U, cylinder diameters D and arm lengths L to explore the space of the parameters Fr, Re and l.

Data of measured amplitudes A and frequencies f obtained for a fixed value of l are shown in figure 7. The uncertainty in the measurements is here mainly due to N. Note that the error bars are smaller than the scatter in the data. They will not be shown in the following figures since the scatter is sufficient to represent this uncertainty.

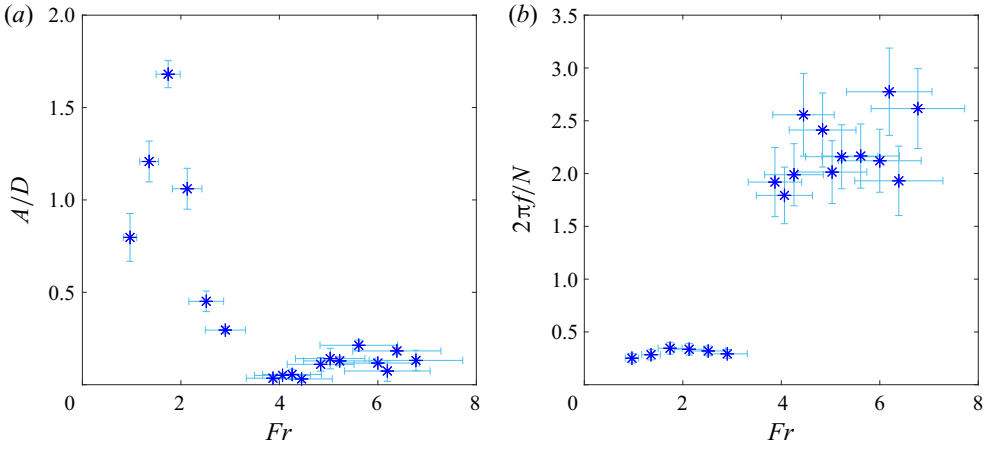

Figure 7. Amplitude (*a*) and frequency (*b*) of the cylinder oscillations with error bars as a function of the Froude number for one set of cylinder diameter and length of arms (Experiment number 12, $N = 1.07 \pm 0.15$ rad s^{-1}, for further information see table 1).

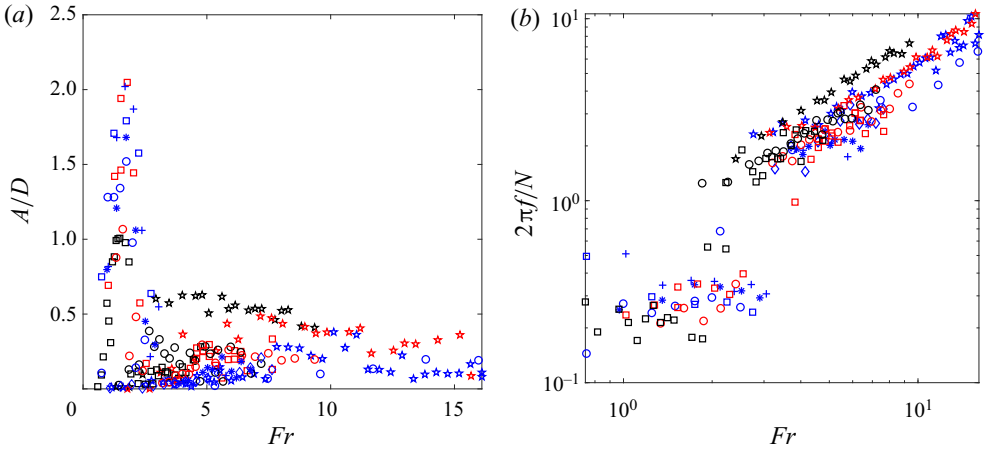

Figure 8. Amplitude (*a*) and frequency (*b*) of the cylinder oscillations as a function of the Froude number for all l considered. Black, red and blue symbols stand for the larger, intermediate and smallest cylinder diameters, respectively (see table 1). Only experiments with amplitude oscillations larger than $0.03D$ are plotted.

Figure 7 shows that, as Fr increases, the cylinder firstly exhibits large-amplitude vibrations at low frequency (with an amplitude peak around $Fr = 1.5$). Then, the oscillations almost disappear before increasing again, to a lesser extent, while their frequency jumps to a value about six times their initial one. This indicates the existence of two distinct vibration modes.

These two modes are also clearly visible in figure 8, where we plot the measured frequencies and amplitudes for all studied l as a function of Fr.

For visibility reasons, only measurements for which the oscillation amplitude was larger than $0.03D$ are kept in the frequency graph. This amplitude threshold has also been applied to all the following frequency plots, except the final ones of § 6.

The large amount of data extending from low Fr, less than one, up to $Fr \sim 16$ enables us to better identify the two frequency modes already spotted on figure 7. The first mode has a low frequency of order $0.25N/2\pi$. It is obtained for small Froude numbers between 1 and 3 and is favoured by large l. The second mode has a higher frequency that increases with U.

Concerning the amplitudes of the modes, the first one has an amplitude as large as $2D$. It corresponds to the peak observed for low Froude numbers in figure 8(a). The second mode exhibits non-negligible amplitudes up to $0.6D$ for larger Froude numbers. The amplitude graph shows a strong scatter in the data, especially at intermediate Froude numbers between 2 and 6, where the system seems to switch from one mode to the other.

In the next two sections, a focus is made on each frequency branch to detail the observations and provide some physical interpretations.

4. The VIV analogous mode

The high-frequency mode is firstly considered. The objective is to show that it can be understood thanks to the models developed in classical VIV theory. For this purpose, a simple mathematical model is derived to estimate the natural frequency f_n of the mechanical system.

The model is based on the application of the momentum equation to the cylinder assuming that the forces acting on the rod can be neglected (small mass, negligible drag). For a cylinder of density ρ_s, volume V_s, diameter D and length L_y, supported by a rigid rod of length L which makes an angle θ with respect to the horizontal plane (see figure 9), the following forces acting on the cylinder can be listed:

(i) Rod's tightness $\boldsymbol{F_T}$.
(ii) Weight $\boldsymbol{F_w} = \rho_s V_s \boldsymbol{g}$.
(iii) Buoyancy force $\boldsymbol{F_b} = -\rho(\theta) V_s \boldsymbol{g}$.
(iv) Drag force $\boldsymbol{F_D} = -\frac{1}{2}\rho(\theta) D L_y C_D U_{abs} \boldsymbol{U_{abs}}$.
(v) Lift force $\boldsymbol{F_L} = -\frac{1}{2}\rho(\theta) D L_y C_L U_{abs} (\boldsymbol{e_y} \wedge \boldsymbol{U_{abs}})$.
(vi) Added mass force $\boldsymbol{F_a} = -C_A \rho(\theta) V_s L(\ddot{\theta}\boldsymbol{e_\theta} - \dot{\theta}^2 \boldsymbol{e_r})$.
(vii) Ball bearing damping $\boldsymbol{F_d} = -cL\dot{\theta}\boldsymbol{e_\theta}$.

Here, C_D and C_L denote the drag and lift coefficients, respectively, C_A the added mass coefficient for a circular cylinder and $\rho(\theta) = \rho_0(1 - N^2 L \sin(\theta)/g)$ the density of the ambient fluid at the cylinder position. Assuming the cylinder at rest when $\theta = 0$, one has $\rho_s = \rho_0$. Figure 9 shows these forces and their orientations. The absolute velocity $\boldsymbol{U_{abs}}$ is the effective velocity of the cylinder due to the combined action of its translation by the trolley and its rotation around the ball bearing caused by oscillations, so that $\boldsymbol{U_{abs}} = -U\boldsymbol{e_x} + L\dot{\theta}\boldsymbol{e_\theta}$. By definition, the drag force is oriented in the direction of $-\boldsymbol{U_{abs}}$ while the lift force is perpendicular to it.

The drag coefficient C_D is considered constant and equal to 1, which is the value for a static cylinder and for Reynolds numbers between 10^3 and 10^4 (von Wieselsberger 1921; Blevins 1984). The drag coefficient varies when the cylinder oscillates (Khalak & Williamson 1996, 1999) but its mean value is found to remain not far from 1, as observed experimentally (Bishop & Hassan 1964; Yamamoto & Nath 1976; Bearman *et al.* 1985), and numerically for low Reynolds numbers (Guilmineau & Queutey 2002; Zheng & Zhang 2008; Placzek, Sigrist & Hamdouni 2009). Sarpkaya (1978) proposed the law $C_D/C_{D0} = 1 + 2A/D$ where C_{D0} denotes the drag value for a fixed cylinder. This formula

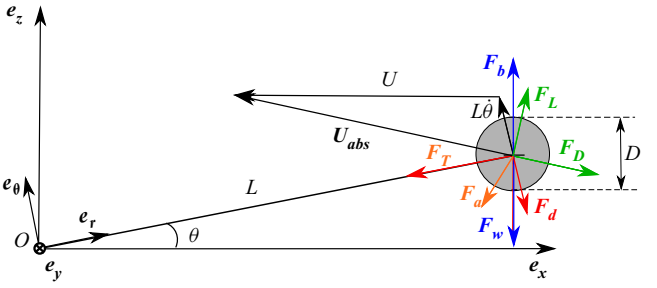

Figure 9. Schematic of the problem. Opposite or perpendicular forces are coloured by pair to ease comprehension.

seems to be confirmed by Khalak & Williamson (1999), especially for low mass ratios. The present VIV-like mode amplitudes mainly lie between $0.1D$ and $0.6D$, so this effect may double the value of C_D for the largest amplitudes. As will be shown, this induces a change lower than 40 % of the predicted frequency, which is smaller than the uncertainties and the scatter in the data. For this reason, we have neglected this effect and chosen a fixed and constant value $C_D = 1$ for the present study.

Applying the operation $\boldsymbol{e_r}\times$ to the momentum equation leads to the angular momentum equation

$$V_s(\rho_0 + \rho C_A)L\ddot{\theta} + cL\dot{\theta} = \frac{F_D}{U_{abs}}[U\sin(\theta) + L\dot{\theta}] - \frac{F_L}{U_{abs}}U\cos(\theta) + (\rho_0 - \rho)V_s g\cos(\theta). \tag{4.1}$$

By assuming $\theta \ll 1$ (in light of experimental observations), $C_A = 1$, keeping only the first-order terms, and switching from θ to $z = L\theta$, the following equation is obtained:

$$\ddot{z} + \left(\frac{c}{2\rho_0 V_s} + \frac{C_D U}{\pi D}\right)\dot{z} + \left(\frac{N^2}{2} + \frac{C_D U^2}{\pi LD}\right)z = \frac{C_L U^2}{\pi D}. \tag{4.2}$$

This is the classical equation of a forced damped oscillator, that is forced by the fluctuating lift and damped by ball bearings and drag force.

Equation (4.2) shows that the restoring forces due to drag and stratification combine to create an oscillator of natural frequency

$$f_n = \frac{1}{2\pi}\sqrt{\frac{N^2}{2} + \frac{C_D U^2}{\pi LD}}. \tag{4.3}$$

This formula applies to both homogeneous and stratified cases.

In the absence of stratification, the natural frequency is

$$f_{n0} = (U/2\pi D)\sqrt{C_D/\pi l}. \tag{4.4}$$

The non-dimensional velocity

$$U^* = \frac{U}{f_n D} \tag{4.5}$$

that is commonly used in VIV studies (Williamson & Govardhan 2004), is thus constant and equal to

$$U_0^* = 2\pi^{3/2}\sqrt{l/C_D}. \tag{4.6}$$

In experiment number 7 (table 1), one can calculate $U_0^* \approx 21.5$. This value is very large compared to the value $1/St = 5$ where high-amplitude VIV oscillations are expected in the classical theory (see § 1). In other words, the natural mechanical frequency and the vortex-shedding frequency are both proportional to the velocity, which implies that they never match for any velocity. It follows that no resonance is possible and no significant oscillations are thus expected in the homogeneous system, which is in agreement with what has been observed in figure 6.

Coming back to the stratified case, the full natural frequency given by (4.3) is analogous to the usual VIV one $(1/2\pi)\sqrt{k/m}$ for spring mounted cylinders, but with the constant stiffness k replaced by a more complex coefficient, depending on U and combining stratification and geometric effects. This frequency can also be written as

$$f_n = \frac{U}{2\pi D}\sqrt{\frac{1}{2Fr^2} + \frac{C_D}{\pi l}}. \tag{4.7}$$

The restoring force is due to the combined action of drag and stratification. The natural frequency of the system is thus no longer proportional to U as for the non-stratified case. Furthermore, for strong stratification f_n becomes constant $f_n \sim N/(2\sqrt{2}\pi)$.

In the general case, the expression of U^* is

$$U^* = \frac{2\pi}{\sqrt{\dfrac{1}{2Fr^2} + \dfrac{C_D}{\pi l}}}. \tag{4.8}$$

This value is bounded by U_0^* that is reached for large Froude number. In table 1, the value of U_0^* has been indicated for each experimental configuration.

Equation (4.2) provides the natural frequency f_n but also the oscillator damping rate σ_D as

$$\sigma_D = \frac{1}{2}\left(\frac{c}{2\rho_0 V_s} + \frac{C_D U}{\pi D}\right). \tag{4.9}$$

Measures in still air demonstrate that the damping rate caused by the structure $(c/(2\rho_0 V_s) \approx 5 \times 10^{-3}\ \mathrm{s}^{-1})$ is at least 20 times smaller than the drag-induced hydrodynamic damping term $(C_D U/(\pi D) \geqslant 0.1\ \mathrm{s}^{-1})$. The value of σ_D thus reduces to the second term in (4.9). The damping ratio $\zeta = \sigma_D/(2\pi f_n)$ is thus close to $U^*/4\pi^2$, and therefore always smaller than $U_0^*/4\pi^2$ which is at most equal to 1.

In figure 10(*a*), f/f_n is plotted vs Fr. One can see that the upper branch mode now exhibits a constant frequency around $2f_n$, which confirms the link between the observed frequency and the natural frequency of the oscillator.

This result is also in good agreement with the formula (1.3) for the lock-in frequency of the lower branch VIV mode which predicts $f^*_{lower} \approx 2.1$ in the case of low mass ratio. This is clearly visible in figure 10(*b*), where this value of the theoretical frequency f^*_{lower} has been indicated with the dashed line. In this figure, where f/f_n is plotted vs U^*, the vortex shedding frequency is also shown by the solid line. A synchronization on the right side of this line is observed, as expected, but for larger values of U^* than in classical VIV theory. The large extent of the synchronization range (until $U^* \approx 35$) is classical for low-mass-ratio experiments, e.g. Govardhan & Williamson (2000) predict a lock-out in homogeneous fluids at $U^* \approx 19$ in the case $m^* = 1$. Note that the observed 'late-U^*' synchronization can be explained by the presence of the second oscillation mode (discussed in next § 5) present at small U^*. It is also not in contradiction to the value of

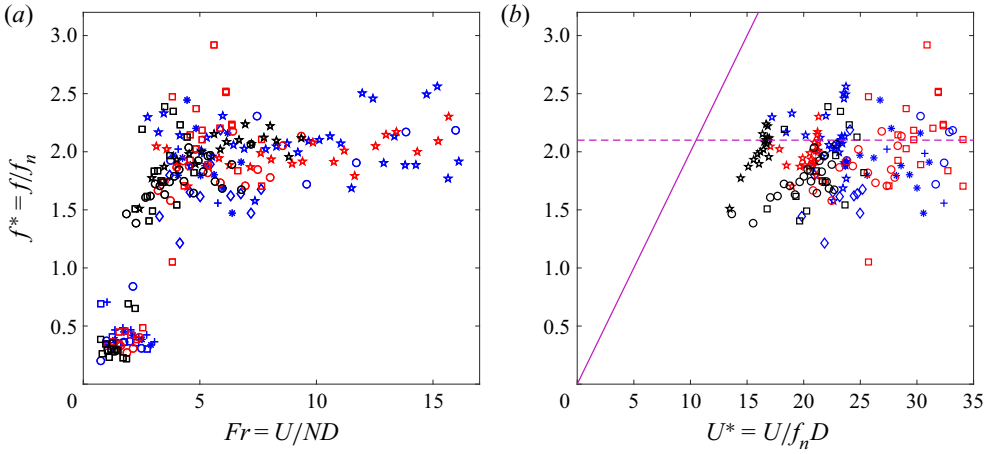

Figure 10. Frequency of VIV mode as a function of Froude number (*a*) and U^* (*b*). Purple line stands for the Strouhal frequency ($St = 0.2$). Purple dotted line stands for f^*_{lower} as defined in (1.3). In (*b*) the lower-frequency mode was removed for clarity.

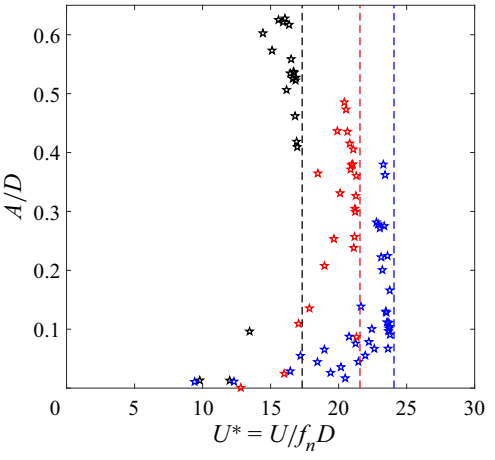

Figure 11. Amplitude of VIV mode as a function of U^*, for experiments with smaller l.

the damping ratio ζ which remains smaller than 1 for all the regimes where oscillations are observed.

In figure 11, the amplitude of the most unstable configurations is plotted as a function of U^*. These configurations correspond to the smallest values of l, for which the maximal value U^*_0 of U^* is also the smallest. These limits are indicated as vertical dashed lines in the figure. The value of the peak amplitude decreases as U^* increases, as expected. But very low amplitudes are also observed for small U^* that cannot be explained by the classical VIV theory. It is suspected that, in this regime, for which the Froude number is small, the stratification modifies the flow and the drag and lift forces it exerts on the cylinder.

5. The galloping mode

5.1. *Description and interpretation*

Below the VIV-like frequency branch, figure 8 shows the existence of a second vibration mode of the system with a constant frequency around $0.25N/2\pi$. This mode occurs at rather low Froude numbers ($Fr \in [1; 3]$), i.e. when the buoyancy forces are no longer negligible with respect to the inertial forces. Furthermore, it is not observed for small arms, but only when the ratio l is larger than a critical value (approximately 7), as will be further discussed in the next section. This indicates that the predominance of buoyancy forces over restoring drag forces is also probably important to observe this mode.

The amplitude of this mode is plotted in figure 12. Despite a strong scatter, the amplitude peak reaches values between one and two cylinder diameters. This is between two and four times the maximal value obtained for VIV modes (see figure 7 and compare figures 11 and 12).

The characteristics of this mode (low-frequency and high-amplitude oscillations) is representative of galloping mode, which occurs in a homogeneous fluid when the axisymmetry of the object is broken. As shown, for example, by Bokaian & Geoola (1984) in the case of a square cylinder, the galloping mode results from an instability: due to symmetry breaking, a tilt of the cylinder induces a lift in the same direction as the motion, and therefore increases the displacement. This instability leads to very large-amplitude oscillations because they are only limited by the structure itself. Owing to its axisymmetry, no galloping instability appears for a circular cylinder in a homogeneous fluid. However, in the presence of stratification, as the axisymmetry is automatically broken, a destabilizing lift could *a priori* be generated, even for a circular cylinder. Numerical simulations are presented in the next section to test this possibility.

5.2. *Numerical simulations*

Numerical simulations are performed using the commercial software COMSOL©. The following configuration is simulated: in a fluid with a linear stratification $\bar{\rho}$, a cylinder is moved at a constant speed $\boldsymbol{U}$, in a direction that makes an angle α with respect to the horizontal plane. The total density is written as $\rho = \rho_0 + \bar{\rho}(z) + \rho'(x, y, z, t)$ where $\rho_0 + \bar{\rho}(z)$ is the background fluid density and ρ' the density induced by the cylinder displacement. Distances are non-dimensionalized by D, velocities by U, pressure by $\rho_0 U^2$ and density by $\rho_0 DN^2/g$. In the cylinder frame of reference, the Navier–Stokes equations under the Boussinesq approximation and the density transport equation can then be written as

$$\frac{\mathrm{D}\boldsymbol{u}}{\mathrm{D}t} = -\nabla p + \frac{1}{Re}\Delta \boldsymbol{u} - \frac{\rho'}{Fr^2}\boldsymbol{e_z}, \tag{5.1a}$$

$$\frac{\mathrm{D}\rho'}{\mathrm{D}t} - (u_z + \sin\alpha) = \frac{1}{ReSc}\Delta\rho'. \tag{5.1b}$$

In (5.1*b*), the u_z term comes from the density transport due to the linear gradient, and the $\sin\alpha$ term is associated with the change of frame.

The problem is solved in a (x, z) domain defined by $-5 \leqslant x \leqslant 20$ and $-5 \leqslant z \leqslant 5$ with the cylinder centred at the origin. The angled velocity is imposed at the top ($z = 5$), the bottom ($z = -5$) and the entrance ($x = -5$) of the domain. Outlet boundary conditions are imposed at $x = 20$. Smooth sponge layers of thickness 1 have been added at the top and bottom in order to damp internal waves: the viscosity is multiplied by a factor 1000 in these layers. A small Froude number $Fr = 1.5$ and an intermediate Reynolds number

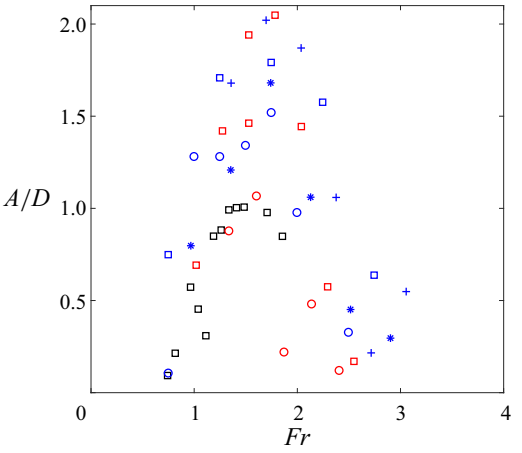

Figure 12. Amplitude of cylinder oscillation in galloping mode as a function of Froude number.

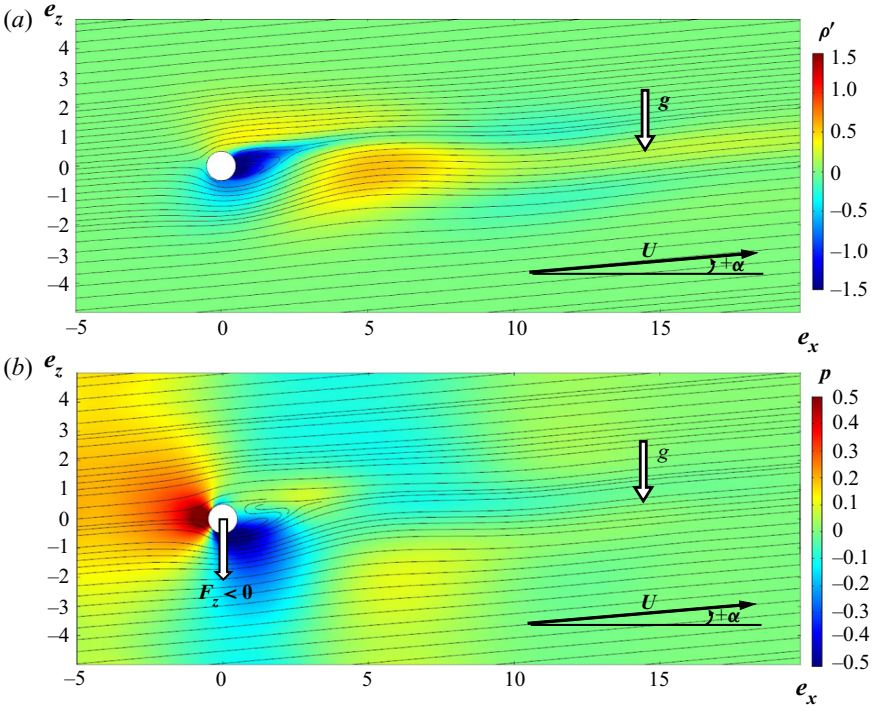

Figure 13. Properties of the stationary perturbation induced by an inclined displacement of the cylinder. $\alpha = 5^\circ$, $Fr = 1.5$, $Re = 300$, $Sc = 1$. (*a*) Density field (colour map) and streamlines. (*b*) Pressure field (colour map) and streamlines.

($Re = 300$) are considered such that there is no vortex shedding (Boyer *et al.* 1989). We are interested in the stationary solution to (5.1*a*,*b*).

The density and pressure fields of this stationary solution are plotted in figure 13. The resulting vertical force (sum of drag and lift components on $\boldsymbol{e}_z$), shown in figure 14, is calculated by integrating the viscous force and pressure force on the cylinder.

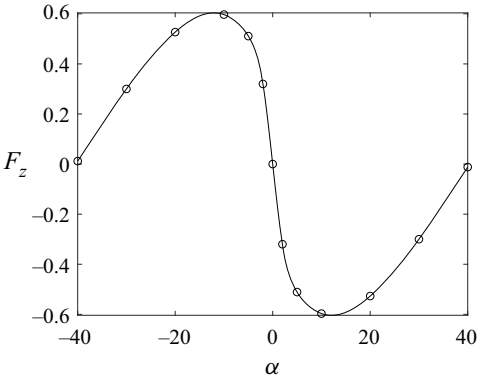

Figure 14. Evolution of the vertical force component F_z as a function of the imposed tilt angle α; $Fr = 1.5$ and $Re = 300$.

Figure 13(a) shows that the density gradient is asymmetrically perturbed by the cylinder. A strong negative lobe of density is created under and behind the cylinder. This density correction is probably related to the combined action of the lee waves and of the recirculation zone. This negative density lobe induces an asymmetric pressure behind the cylinder since its z derivative is equal to the density in the absence of motion. Indeed, although the usual positive pressure lobe causing drag is observed in front of the cylinder, figure 13(b) also demonstrates the presence of a negative pressure on the lower right of the cylinder. This induces a downward lift $F_z < 0$. Since the cylinder is already going down, this lift reinforces the initial motion, thus an instability develops.

The fact that F_z should be negative for small positive α corresponds in our case to the classical Den Hartog criterion for galloping instability (Den Hartog 1932)

$$\frac{\partial C_L}{\partial \alpha} + C_D < 0, \tag{5.2}$$

requiring in fact that $\partial F_z/\partial \alpha$ should be negative at small angles. It can be recovered by developing F_z around small α angles (see Blevins (1977), for further details).

Figure 14 shows that this destabilization process occurs for angles in the range $[-40^\circ, 40^\circ]$. For larger angles, the drag force is stronger than the lift and the destabilizing mechanism described above is no longer present.

To conclude this section, it was shown by analysing the properties of the perturbation induced by the cylinder motion, that the lift can become destabilizing in the presence of stratification when the displacement is no longer horizontal. The mechanism is therefore very similar to the galloping instability.

The next section focuses on the influence of the non-dimensional parameters defined in § 2.3 on the development of the galloping and VIV analogous modes.

6. Competition between the two regimes

As already mentioned, there are three main non-dimensional parameters characterizing the system: the length ratio l which specifies the geometry, the Froude number Fr which compares buoyancy and inertial forces and the Reynolds number Re which characterizes viscous effects. In this section, the influence of these different parameters on the observed mode is evaluated.

All data are plotted as a function of Fr and l in figure 15(a). Each solid circle corresponds to an experiment where a distinct mode has been observed. The colour of the circle is

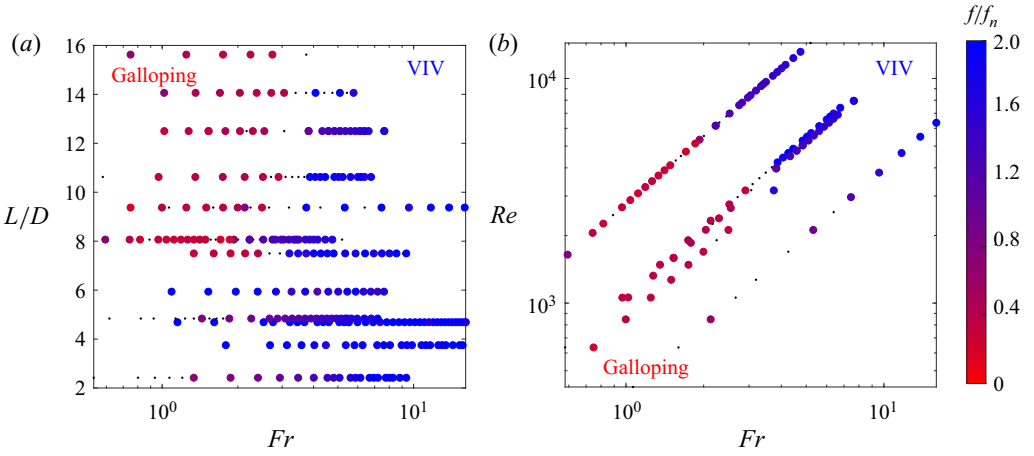

Figure 15. Experimental identification of galloping (in red) and VIV (in blue) modes based on the frequency measurement. Dots stand for performed experiments from which no frequency nor amplitude could be determined. (*a*) Map in (*Fr*, *l*) plane of all data. (*b*) Map in (*Fr*, *Re*) plane of a reduced set of data ($l \in [8, 12.5]$).

related to the frequency of the mode: red circles correspond to low-frequency galloping modes, while blue circles to high-frequency VIV-like modes. This stability map clearly shows that the galloping mode is limited to the square domain of high-l and low-Fr: l must be larger than 7 and Fr below 3 for the galloping mode to appear. However, these data cover a large range of Reynolds numbers.

To evaluate the influence of the Reynolds number, the data are plotted as a function of Fr and Re in figure 15(*b*) for a reduced range of l ($l \in [8, 12.5]$) where both modes are observed. The Reynolds number is found to have a weak impact on the transition between galloping and VIV analogous mode compared to the two other non-dimensional numbers. The transition Froude number between the two modes seems to decrease as the Reynolds number increases. However, it is difficult to quantify precisely the Re dependence due the lack of data. Indeed, at transition, amplitudes are very weak and frequencies difficult to measure, so many experiments were not conclusive, causing a gap in the available data.

Nevertheless, from figure 15, it can be inferred that the two main control parameters of the system are the Froude number and the geometric parameter l. This is in agreement with the model that have been developed. It has indeed been shown that stratification is essential for the appearance of the galloping mode, while the parameter l affects the drag force that is responsible for the development of the VIV-like mode. Viscosity is not expected to play an important role, especially in the regimes of large Re/Fr that have been considered.

7. Conclusion

The classical experiment of a spring-mounted cylinder has been adapted to the case of a stratified fluid: the flowing water channel has been replaced by a towing tank of stratified fluid, and the cylinder has not been mounted on springs but on flat blade-shaped arms free to rotate around their end. With this set-up, drag and buoyancy forces induce a vertical restoring force that mimics the action of a spring.

This pioneered experimental study of FIV in a stratified fluid has brought out the existence of two different oscillating modes for a circular cylinder.

The first one has a moderate amplitude (less than $0.6D$) and a frequency that can be understood by a classical VIV approach. Indeed, it is proportional to the natural

frequency f_n of the mechanical system. The lock-in frequency ratio f/f_n has been shown to be reasonably well predicted by the classical VIV theory for low mass ratio (Williamson & Govardhan 2004). The natural frequency f_n is shown to be not constant. It varies from $f_n \sim N/(2\sqrt{2}\pi)$ for small Froude numbers to $f_n \sim U/2\pi D\sqrt{C_D/\pi l}$ for large Froude numbers. In a spring-mounted experiment, this natural frequency would be expected to switch from $f_n \sim N/(2\sqrt{2}\pi)$ to $\sqrt{k/(m^* + C_A)}$ as the spring constant k increases.

The second mode is a galloping mode, characterized by a large amplitude (up to $2D$) and a low frequency close to $0.25N/2\pi$. It has been linked to the breaking of the axisymmetry due to the stratification. In particular, it has been associated with the presence of a destabilizing lift force, as for the galloping modes of non-cylindrical objects. This mode has been observed for low Froude numbers ($Fr \leqslant 3$), and long arms ($l \geqslant 7$).

Galloping and VIV modes were also observed in classical VIV systems in a homogeneous fluid when the object is no longer axisymmetric, but the scenario of appearance is different. In general, as U^* increases, VIV mode appears first, then it is replaced by the galloping mode, that never disappears (Nemes *et al.* 2012; Mannini *et al.* 2014). Here, the scenario is opposite. We have first observed the galloping mode for small U^* and then the VIV-like mode. This can be understood because small values of U^* also correspond to small Froude numbers, which are necessary for the existence of the galloping mode. As U^* increases, Fr also increases, so the buoyancy restoring force responsible for the instability of the galloping mode reduces, and is finally not sufficient to sustain the mode when Fr is too large.

The effect of the Reynolds number on the transition from one mode to the other has been analysed for Re between 500 and 15 000, but no significant dependence has been noticed.

Oceans, which are stratified, are full of cables (transatlantic communications, oil platforms...) subject to complex streams, and then, potentially, the FIV phenomenon. As this study shows a strong influence of stratification on fluid–structure interactions that has never been addressed before, it would be of interest to consider these specific applications. In oceans and seas, the Brünt–Väisälä frequency N ranges from 10^{-3} in the deep ocean (Munk 1966) to 1.5×10^{-2} rad s^{-1} in the thermocline of the black sea, for example (Capet *et al.* 2016). With the latter value, considering a current of $U = 0.1$ m s^{-1}, cables of diameter D larger than 67 cm have $Fr < 10$. For such a value of the Froude number, a VIV-like mode leading to non-negligible oscillations of the structure has been observed in this study. In the atmosphere, where N is typically of order 2×10^{-2} rad s^{-1} (Bougeault & Sadourny 2001), with a wind of velocity $U = 1$ m s^{-1}, bridge structures of diameter larger than 5 m may undergo oscillations since the Froude number is below 10.

This study suggests numerous possible further research to fully understand the presented modes. Indeed, the VIV model presented here may be improved by considering the increase of the mean drag with the oscillation amplitude. The fluctuating component of the drag and the lift may also need further investigations to better understand the VIV analogous mode.

Exploring the low-l and low-Fr regimes would also be very interesting as these parameters could lead to a VIV-like mode modified by the important variations of the Strouhal number observed for low Fr.

Changing parameters such as the inclination angle, the rigidity of the body and analysing the effect of a nonlinear stratification would be interesting in order to perform research closer to real-life systems. Another set-up with springs could also be useful for a better comparison with classical homogeneous VIV results, and to ease results interpretation by separating geometric and flow parameters. Finally, using numerical simulations to explore

regimes difficult to reach experimentally, such as low Froude and Reynolds number regimes, could be another interesting research path.

Acknowledgements. The authors would like to thank T. Leweke for fruitful discussions.

Declaration of interests. The authors report no conflict of interest.

Author ORCIDs.
Sarah Christin https://orcid.org/0000-0002-9836-9396;
Patrice Meunier https://orcid.org/0000-0002-5034-6056;
Stéphane Le Dizès https://orcid.org/0000-0001-6540-0433.

References

Assi, G.R.S., Bearman, P.W. & Meneghini, J.R. 2010 On the wake-induced vibration of tandem circular cylinders: the vortex interaction excitation mechanism. *J. Fluid Mech.* **661**, 365–401.

Bearman, P.W., Downie, M.J., Graham, J.M.R. & Obasaju, E.D. 1985 Forces on cylinders in viscous oscillatory flow at low Keulegan–Carpenter numbers. *J. Fluid Mech.* **154**, 337–356.

Bearman, P.W. 1984 Vortex shedding from oscillating bluff bodies. *Annu. Rev. Fluid Mech.* **16** (1), 195–222.

Bernitsas, M.M., Raghavan, K., Ben-Simon, Y. & Garcia, E.M.H. 2008 VIVACE (Vortex induced vibration aquatic clean energy): a new concept in generation of clean and renewable energy from fluid flow. *Trans. ASME: J. Offshore Mech. Arctic Engng* **130** (4), 041101.

Bishop, R.E.D. & Hassan, A.Y. 1964 The lift and drag forces on a circular cylinder oscillating in a flowing fluid. *Proc. R. Soc. Lond.* A **277** (1368), 51–75.

Blevins, R.D. 1977 *Flow-Induced Vibration*. Van Nostrand Reinhold Co. p. 377.

Blevins, R.D. 1984 *Applied Fluid Dynamics Handbook*. Van Nostrand Reinhold.

Bokaian, A.R. & Geoola, F. 1984 Hydroelastic instabilities of square cylinders. *J. Sound Vib.* **92** (1), 117–141.

Bosco, M. 2015 Etude du sillage stratifié d'un cylindre. PhD thesis, Aix-Marseille.

Bougeault, P. & Sadourny, R. 2001 *Dynamique de l'atmosphère et de l'océan*. Editions Ecole Polytechnique.

Boyer, D.L., Davies, P.A., Fernando, H.J.S. & Zhang, X. 1989 Linearly stratified flow past a horizontal circular cylinder. *Phil. Trans. R. Soc. Lond.* A **328** (1601), 501–528.

Browand, F.K. & Winant, C.D. 1972 Blocking ahead of a cylinder moving in a stratified fluid: an experiment. *Geophys. Fluid Dyn.* **4** (1), 29–53.

Capet, A., Stanev, E., Beckers, J.-M., Murray, J. & Grégoire, M. 2016 Decline of the black sea oxygen inventory. *Biogeosciences* **13**, 1287–1297.

Chang, C.-C.J., Kumar, R.A. & Bernitsas, M.M. 2011 VIV and galloping of single circular cylinder with surface roughness at $3.0 \times 10^4 \leqslant Re \leqslant 1.2 \times 10^5$. *Ocean Engng* **38** (16), 1713–1732.

Chashechkin, Y.D. & Voyekov, I.V. 1993 Vortex systems past a cylinder in a continuously stratified fluid. *Izv. Atmos. Ocean. Phys.* **29**, 787–787.

Coutanceau, M. & Bouard, R. 1977 Experimental determination of the main features of the viscous flow in the wake of a circular cylinder in uniform translation. Part 1. Steady flow. *J. Fluid Mech.* **79** (2), 231–256.

De Wilde, J.J., Huijsmans, H.M. & Triantafyllou, M.S. 2003 Experimental investigation of the sensitivity to in-line motions and magnus-like lift production on the vortex-induced vibrations. In *The Thirteenth International Offshore and Polar Engineering Conference*, pp. 593–598. International Society of Offshore and Polar Engineers.

Den Hartog, J.P. 1932 Transmission line vibration due to sleet. *Trans. Am. Inst. Elect. Engrs* **51** (4), 1074–1076.

Den Hartog, J.P. 1954 Recent technical manifestations of Von Kármán's vortex wake. *Proc. Natl Acad. Sci. USA* **40** (3), 155.

Feng, C.C. 1968 The measurement of vortex induced effects in flow past stationary and oscillating circular and d-section cylinders. PhD thesis, University of British Columbia.

Govardhan, R. & Williamson, C.H.K. 2000 Modes of vortex formation and frequency response of a freely vibrating cylinder. *J. Fluid Mech.* **420**, 85–130.

Graebel, W.P. 1969 On the slow motion of bodies in stratified and rotating fluids. *Q. J. Mech. Appl. Maths* **22** (1), 39–54.

Griffin, O.M. 1985 Vortex-induced vibrations of marine cables and structures. *Tech. Rep.* 5600. Naval Research Lab., Washington D.C.

GROUTHIER, C., MICHELIN, S., BOURGUET, R., MODARRES-SADEGHI, Y. & DE LANGRE, E. 2014 On the efficiency of energy harvesting using vortex-induced vibrations of cables. *J. Fluids Struct.* **49**, 427–440.
GUILMINEAU, E. & QUEUTEY, P. 2002 A numerical simulation of vortex shedding from an oscillating circular cylinder. *J. Fluids Struct.* **16** (6), 773–794.
HONJI, H. 1988 Vortex motions in stratified wake flows. *Fluid. Dyn. Res.* **3** (1–4), 425.
HWANG, R.R. & LIN, S.H. 1992 On laminar wakes behind a circular cylinder in stratified fluids. *J. Fluids Engng* **114** (1), 20–28.
KHALAK, A & WILLIAMSON, C.H.K. 1996 Dynamics of a hydroelastic cylinder with very low mass and damping. *J. Fluids Struct.* **10** (5), 455–472.
KHALAK, A. & WILLIAMSON, C.H.K. 1997 Investigation of relative effects of mass and damping in vortex-induced vibration of a circular cylinder. *J. Wind Engng Ind. Aerodyn.* **69**, 341–350.
KHALAK, A. & WILLIAMSON, C.H.K. 1999 Motions, forces and mode transitions in vortex-induced vibrations at low mass-damping. *J. Fluids Struct.* **13** (7–8), 813–851.
LIENHARD, J.H. 1966 *Synopsis of lift, drag, and vortex frequency data for rigid circular cylinders*, vol. 300. Technical Extension Service, Washington State University Pullman, WA.
LIN, J.-T. & PAO, Y.-H. 1979 Wakes in stratified fluids. *Annu. Rev. Fluid Mech.* **11** (1), 317–338.
MANNINI, C., MARRA, A.M. & BARTOLI, G. 2014 VIV–galloping instability of rectangular cylinders: review and new experiments. *J. Wind Engng Ind. Aerodyn.* **132**, 109–124.
MANNINI, C., MARRA, A.M., MASSAI, T. & BARTOLI, G. 2016 Interference of vortex-induced vibration and transverse galloping for a rectangular cylinder. *J. Fluids Struct.* **66**, 403–423.
MEUNIER, P. 2012 Stratified wake of a tilted cylinder. Part 1. Suppression of a von Kármán vortex street. *J. Fluid Mech.* **699**, 174–197.
MUNK, W.H. 1966 Abyssal recipes. In *Deep Sea Research and Oceanographic Abstracts*, vol. 13, pp. 707–730. Citeseer.
NAKAMURA, Y., HIRATA, K. & KASHIMA, K. 1994 Galloping of a circular cylinder in the presence of a splitter plate. *J. Fluids Struct.* **8** (4), 355–365.
NEMES, A., ZHAO, J., LO JACONO, D. & SHERIDAN, J. 2012 The interaction between flow-induced vibration mechanisms of a square cylinder with varying angles of attack. *J. Fluid Mech.* **710**, 102–130.
OHYA, Y., UCHIDA, T. & NAGAI, T. 2013 Near wake of a horizontal circular cylinder in stably stratified flows. *Open J. Fluid Dyn.* **3**, 311–320.
PARKINSON, G.V. & WAWZONEK, M.A. 1981 Some considerations of combined effects of galloping and vortex resonance. *J. Wind Engng Ind. Aerodyn.* **8** (1–2), 135–143.
PLACZEK, A., SIGRIST, J.-F. & HAMDOUNI, A. 2009 Numerical simulation of an oscillating cylinder in a cross-flow at low Reynolds number: forced and free oscillations. *Comput. Fluids* **38** (1), 80–100.
ROSHKO, A. 1961 Experiments on the flow past a circular cylinder at very high Reynolds number. *J. Fluid Mech.* **10** (3), 345–356.
SARPKAYA, T. 1978 Fluid forces on oscillating cylinders. *STIA* **104**, 275–290.
SARPKAYA, T. 2004 A critical review of the intrinsic nature of vortex-induced vibrations. *J. Fluids Struct.* **19** (4), 389–447.
SONG, R., SHAN, X., LV, F. & XIE, T. 2015 A study of vortex-induced energy harvesting from water using PZT piezoelectric cantilever with cylindrical extension. *Ceram. Intl* **41**, S768–S773.
STROUHAL, V. 1878 Über eine besondere art der tonerregung. *Ann. Phys.* **241** (10), 216–251.
TRITTON, D.J. 2012 *Physical Fluid Dynamics*. Springer Science & Business Media.
VON KARMAN, T. 1911 Über den mechanismus des widerstandes, den ein bewegter körper in einer flüssigkeit erfährt. *Nachr. Ges. Wiss. Göttingen* **1911**, 509–517.
VON WIESELSBERGER, C. 1921 Neuere feststellungen uber die gesetze des flussigkeits und luftwiderstands. *Phys. Z.* **22**, 321.
WILLIAMSON, C.H.K. 1996*a* Three-dimensional wake transition. *J. Fluid Mech.* **328**, 345–407.
WILLIAMSON, C.H.K. 1996*b* Vortex dynamics in the cylinder wake. *Annu. Rev. Fluid Mech.* **28** (1), 477–539.
WILLIAMSON, C.H.K. & GOVARDHAN, R. 2004 Vortex-induced vibrations. *Annu. Rev. Fluid Mech.* **36**, 413–455.
YAMAMOTO, T. & NATH, J.H. 1976 High Reynolds number oscillating flow by cylinders. *Coast. Engng* **1** (15), 135.
ZHENG, Z.C. & ZHANG, N 2008 Frequency effects on lift and drag for flow past an oscillating cylinder. *J. Fluids Struct.* **24** (3), 382–399.